Depletion of surface accumulation charge in InN by anodic oxidation

A. Denisenko,[1,a)] C. Pietzka,[1] A. Chuvilin,[2] U. Kaiser,[2] H. Lu,[3] W. J. Schaff,[3] and E. Kohn[1]

[1]*Institute of Electron Devices and Circuits, Ulm University, Ulm 89069, Germany*
[2]*Electron Microscopy Group of Materials Science, Ulm University, Ulm 89069, Germany*
[3]*Department of Electrical and Computer Engineering, Cornell University, Ithaca, New York 14853-2201, USA*

(Received 18 July 2008; accepted 17 December 2008; published online 3 February 2009)

Si-doped InN layer by molecular beam epitaxy was subjected to anodic oxidation in 0.1 M potassium hydroxide (KOH) electrolyte and characterized by electrochemical methods to derive carrier profile at the InN surface. The obtained results were compared to the characteristics of a planar resistor structure and vertical metal-oxide-semiconductor (MOS) diodes with Ni-metal contacts on the oxidized InN. Both measurements in electrolyte and in air confirmed the formation of a surface oxide layer after the anodic treatment and depletion of the surface accumulation charge of the as-grown InN. The upward band bending of InN at the oxide interface was also concluded from the analysis of capacitance-voltage characteristics of the MOS diodes. Transmission electron microscopy revealed a nonuniform oxide layer containing porelike structures of a few nanometers in diameter. © *2009 American Institute of Physics*. [DOI: 10.1063/1.3073930]

I. INTRODUCTION

The low-bandgap semiconductor indium nitride has recently attracted much attention due to the existence of an electron accumulation layer on its surface, which causes a downward bending of the conduction band by ~0.9 eV.[1–4] The carrier density within this accumulation layer has been estimated to be in the range of 2×10^{13} cm^{-2}.[1,4] The origin of the surface charge has been explained by a donor-type surface state located in the conduction band of wurtzite InN material.[5] Although the surface accumulation effect might be interesting for InN-based chemical sensors,[6,7] it may represent a hurdle for electron devices with metal gates like field effect transistors (FETs). As no rectifying Schottky contact has been demonstrated so far on the as-grown InN, InN-based FET structures still need to use foreign gate insulating materials.[8]

A possible solution for controlling the surface characteristics of InN could be an oxidation, which may induce electronic surface states depleting the surface accumulation layer. The upward bending of the surface band structures upon oxidation has been reported for GaN.[9,10] A partial depletion of the surface accumulation charge density has been reported also for InN subjected to ozone-assisted oxidation.[11,12] The downward bending after such a treatment has been reduced to less than 0.4 eV.[11] This surface depletion effect has been related to formation of indium-oxide surface bonds, which have passivated the surface donors. However, the oxidation-induced band bending of the InN surface has been found strongly dependent on the applied treatment. For instance, thermal oxidation at temperatures between 200 and 600 °C did not induce the expected depletion, but instead increased the surface carrier accumulation.[11] A similar accumulation effect has been reported also for the case of epitaxial growth of indium oxide on InN.[12]

A more reliable process could be anodic oxidation in an electrolyte, which has been already demonstrated for other nitride-based semiconductors and heterostructures.[10,13,14] In Ref. 10 it has been shown that photoelectrochemical oxidation of GaN resulted in a metal-oxide-semiconductor (MOS)-like structure with negative charge at the oxide/GaN interface. This interface charge induced an upward band bending at the GaN surface. Also, it has been shown that the anodic treatment of lattice-matched InAlN/GaN heterostructures resulted in a depletion of the polarization-induced two-dimensional electron gas at the InAlN/GaN interface, which has been explained by the formation of a surface oxide layer with electronic states at the oxide/InAlN interface.[14]

The electrochemically induced oxidation has been already applied for polycrystalline InN.[15] This treatment has resulted in the formation of surface oxide groups, which have induced a *p*H sensitivity of the surface potential close to the theoretical limit of 59 mV/pH (Nernst's law), which could be interesting for chemical sensing. However, no data on the electronic characteristics of the oxidized InN surface have been presented so far.

In this report we describe the effect of anodic oxidation of single-crystalline InN (0001) layers on the surface accumulation charge and the corresponding band bending. The electronic characteristics of the oxidized surface were obtained by the capacitance-voltage (*C-V*) and impedance spectroscopy measurement techniques applied to the InN-electrolyte junction and to metal Schottky diodes fabricated on the oxidized InN surface. Additional data on the oxidation-induced surface charge were obtained by analyzing the planar resistor structures. The morphology of the oxidized surface was analyzed by high resolution transmission electron microscopy (TEM).

[a)]Author to whom correspondence should be addressed. Electronic mail: andrej.denisenko@uni-ulm.de. Tel.: +49 731 502 6177. FAX: +49 731 502 6155.

0021-8979/2009/105(3)/033702/7/$25.00 © 2009 American Institute of Physics

Author complimentary copy. Redistribution subject to AIP license or copyright, see http://jap.aip.org/jap/copyright.jsp

II. EXPERIMENTAL

Si-doped InN layers were grown by molecular-beam epitaxy (MBE) on sapphire substrates with a GaN buffer and an AlN interlayer. Details on the MBE growth can be found elsewhere.[16] The thickness of the InN epilayer was $\sim$0.3 μm. The average carrier concentration within the doped InN layer was 9.6×10^{18} cm^{-3} as determined by Hall effect measurement. The corresponding carrier mobility μ was 650 cm^2/V s at room temperature. The average surface roughness determined by atomic force microscopy was about 10 nm (rms).

Three types of the InN-based structures were prepared for our experiments: (i) electrochemical electrodes, (ii) a planar resistor, and (iii) vertical diodes on the oxidized surface. For the electrochemical experiments, InN samples were mounted on a conductive holder and contacted to the doped InN layer using a conductive silver paste. The electrode structures were passivated by a Teflon®-based adhesive tape with a perforated opening of 1 mm in diameter for the contact with electrolytes. The electrochemical experiments including cyclic voltammetry, electrochemical impedance spectroscopy, and electrolyte-based *C-V* measurements were performed using a potentiostat (PARSTAT 2273, Princeton Applied Research®). These measurements were performed at room temperature using a standard three-electrode glass cell with a platinum counter and a saturated calomel reference electrode (SCE) placed in a grounded Faraday cage with the solutions deaerated by nitrogen gas flow. The same setup was used for anodic oxidation of InN surface in KOH solution (for details, see below). The electrochemical measurements with the as-grown and the oxidized InN electrodes were performed in a neutral buffer solution (pH=7) with KH_2PO_4 and $Na_2H_2P_2O_7$ components (by VWR Int.®) to avoid uncontrolled *in situ* oxidation.

The planar resistor on the InN layer was formed by etching a mesa structure by Ar plasma. The conductive InN layer outside the mesa was etched completely, leaving a mesa of 1×3 mm^2 in size. Then, a part of the mesa was protected by adhesive tape used for the electrode passivation, leaving an open window for anodic oxidation. Both the electrode and the resistor structures were oxidized under the identical conditions.

The anodic oxidation in 0.1 M potassium hydroxide (KOH) electrolyte was performed at a constant potential of about 1–1.5 V versus SCE, which was above the onset of oxygen evolution on the InN surface in this electrolyte. The total charge passed through the electrochemical cell during the oxidation $Q=\int I\times dt$ was about 32 mC/cm^2, which represents a transfer of 2×10^{17} of electrons/cm^2. The oxidation process was controlled by monitoring the optical reflection of the surface under microscope illumination. Similar phenomena have been reported in Ref. 14, where a color change in InN upon anodic treatment was related to the chemisorption of hydroxyl ions.

After the oxidation treatment, a set of metal contacts was fabricated on the oxidized InN surface. The sequence of 50 nm Ni followed by 100 nm Au was deposited using an e-beam assisted evaporation. The metallization was made through a shadow mask to avoid any additional surface treatment by lithography process. The same metallization was also deposited on the nonoxidized area of the InN surface where it showed Ohmic characteristics. The current-voltage (*I-V*) characteristics of the fabricated diode structures were recorded using a HP4145B parameter analyzer. The impedance spectroscopy measurements were performed using a HP4192A impedance analyzer in the frequency range of 1 kHz–10 MHz.

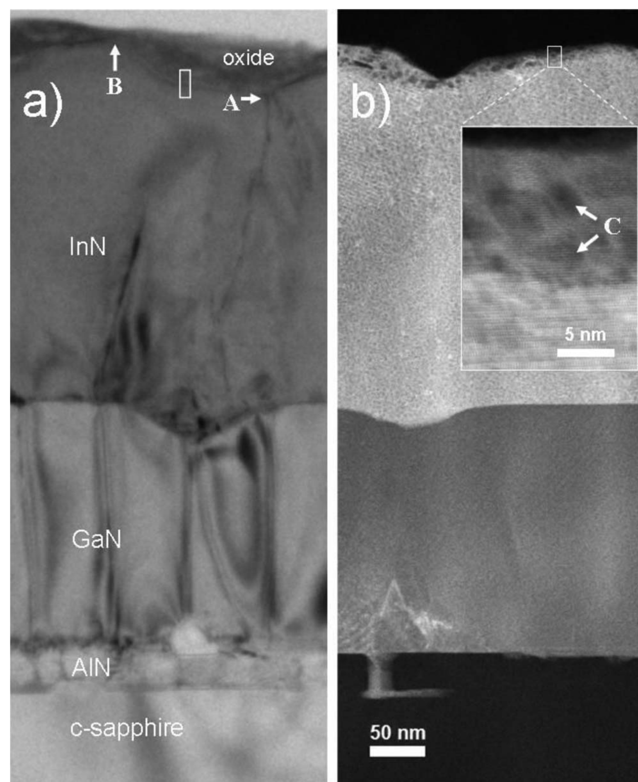

FIG. 1. (a) TEM and (b) high-angle annular dark field STEM images of the Si-doped InN subjected to anodic oxidation. The white frame in (a) shows an approximate location of the interface region shown in Fig. 2.

III. RESULTS AND DISCUSSION

In Sec. III A, we describe at first the results of the TEM analysis of the oxidized InN. This is followed by the analysis of the InN-electrolyte junction of the as-grown state and with oxidized surface. The results of the planar resistor and vertical diodes on the oxidized surface are described in Secs. III D and III E of this paper.

A. Morphology of oxidized InN surface

A cross-sectional TEM image of the epitaxial InN layer after the anodic treatment is shown in Fig. 1(a). It disclosed a nonuniform oxide in thickness and structure. The growth of the oxide layer occurred preferentially in the regions of troughs in the faceted initial surface. This preferential oxidation might be associated with dislocations emerging at these sites [position A in Fig. 1(a)]. The oxide thickness in these areas was varied from 20 to 40 nm. However the oxide layer was formed on the surface facets as well, although with less

Author complimentary copy. Redistribution subject to AIP license or copyright, see http://jap.aip.org/jap/copyright.jsp

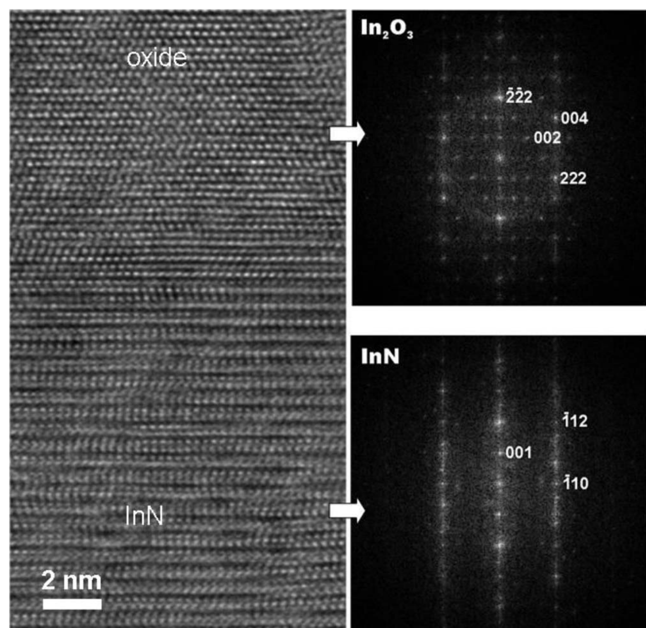

FIG. 2. High resolution TEM image of InN/oxide interface region and FT spectra of the InN and the oxide areas. A complicated net of weak reflections on the spectra of In_2O_3 is most probably due to multiple twinning.

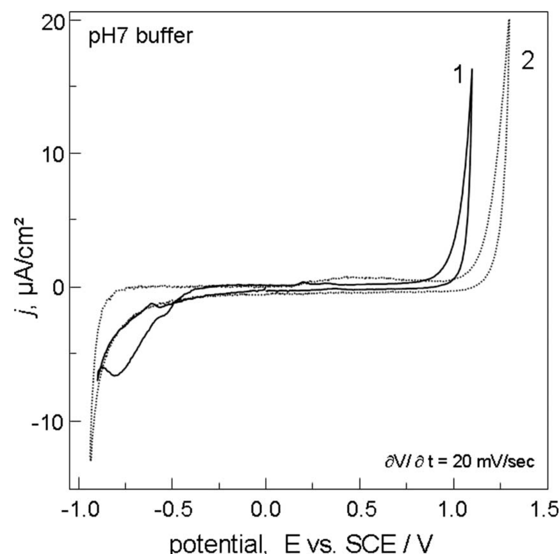

FIG. 3. Liner cyclic voltammetry scans of InN electrode in *p*H 7 buffer solution. Curve 1: as-grown surface; curve 2: after anodic oxidation.

thickness which varied from 5 to 10 nm [position B in Fig. 1(a)]. Thus, no areas of nonoxidized InN remained on the surface after the anodic treatment.

The epitaxial relationship between initial InN phase and the anodic oxide can be revealed in Fig. 2. It shows a high resolution TEM image of the interface and the corresponding Fourier transformation (FT) spectra obtained from the areas of InN and anodic oxide, respectively. The approximate location of the analyzed interface area is marked in Fig. 1(a) by the white frame. The interface between InN and oxide phases was relatively sharp, as is evidenced also by Fig. 1. The FT spectrum of the oxide area revealed reflections of crystalline In_2O_3 phase. A complicated net of weak reflections on the spectra of In_2O_3 is most probably due to multiple twinning.[17] Reflections of In_2O_3 were also present to some extent in the FT spectrum of the wurtzite InN layer. Most probably this is an artifact caused by oxidation of the TEM sample in air.

A scanning TEM (STEM) image in Fig. 1(b) revealed a porelike structure of the produced oxide layer. The porelike features [position C in Fig. 1(b)] varied from 1 to 5 nm in diameter and were observed both at surface facets and in the regions of troughs throughout the entire thickness of the oxide. According to the TEM image, the pores occupied a significant part of the total volume of the oxide layer. In the areas close to the interface with nonoxidized InN, the pores were separated by protrusions of relatively nonattacked material.

Similar porelike structure of oxide has been reported for *n*-type GaN subjected to anodic oxidation under illumination.[18] The exposure to light generated holes in the semiconductor material, leading to full oxidation of gallium atoms and release of nitrogen at the oxide interface.[19] The produced N_2 gas was believed to trap within the oxide layer, thus producing the nonuniform material. In a similar way, the release of nitrogen might be also responsible for the observed porous structure of indium oxide. However the detailed mechanism of such process is not clear yet, especially taking into account that the anodic treatment in our experiments was performed without external illumination.

B. As-grown InN in electrolyte

Prior to oxidation, the as-grown InN layer was analyzed in a buffer electrolyte (pH=7) to verify the electronic characteristics of the surface. The cyclic voltammogram of the as-fabricated InN surface in the buffer solution is shown in Fig. 3, curve 1. It showed a potential window of water electrolytes of ~2 V with no activity except for a cathodic peak around −0.8 V versus SCE prior to the onset of hydrogen evolution. This activity is similar to that of indium[20] or indium phosphide electrodes[21,22] and can be ascribed to the reduction in indium-oxide groups. This indicated that a thin oxide layer had been formed on the as-grown surface most probably due to exposure to air.[23] Therefore, the definition "as-grown surface" is applied here to the surface prior to the anodic oxidation step. The background current of the as-grown InN was ~2 nA/mm^2 within the potential window outside the activity range.

Figure 4(a) shows the impedance spectrum of the as-fabricated electrode at the potential of +0.8 V versus SCE. The impedance data were fitted using ZSIMPWIN® electrochemical data analysis software. The value of a series resistance R_S of the electrochemical cell of 10 $\Omega\,cm^2$ was subtracted from the data prior to the fitting procedure. The fitting parameters are listed in Table I. The impedance data can be modeled with two *RC*-circuits in series, as shown in the inset of Fig. 3(a). For better fit, the second capacitance was replaced by a constant phase element (CPE) with admittance $Y_{CPE}=Q_0(j2\pi f)^n$, where f is the frequency. The dispersion factor n from the fit was about 0.97, which was very close to an ideal capacitance ($n=1$). The first *RC*-circuit (R_1C_1) with a bias-dependent C_1 can be ascribed to the doped indium nitride. The corresponding resistance R_1 was in the range of 10 $M\Omega\,cm^2$, which confirmed the high quality of the mate-

Author complimentary copy. Redistribution subject to AIP license or copyright, see http://jap.aip.org/jap/copyright.jsp

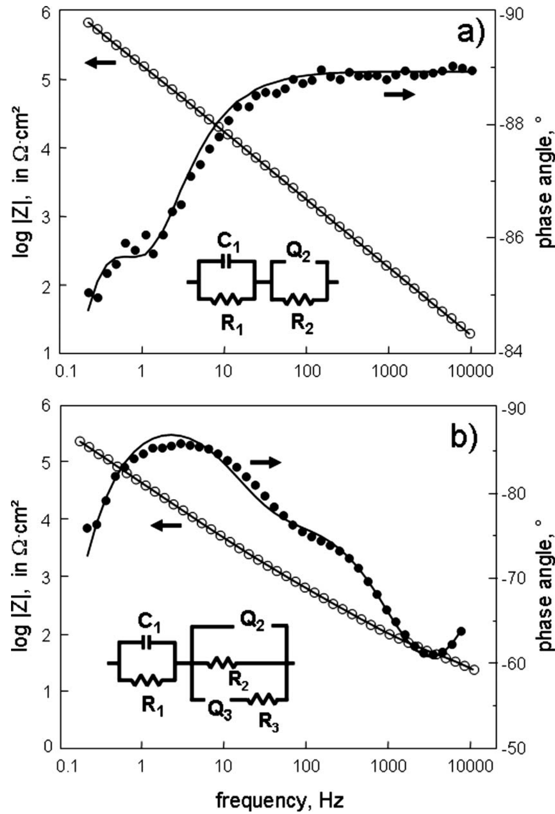

FIG. 4. Bode plots of the electrochemical impedance spectroscopy measurements (symbols) of InN electrode in *p*H 7 buffer solution at the potential of +0.8 V vs SCE. (a) As-grown surface; (b) after anodic oxidation. The solid curves show the fits using the equivalent circuits depicted in the insets. The fitting parameters are listed in Table I.

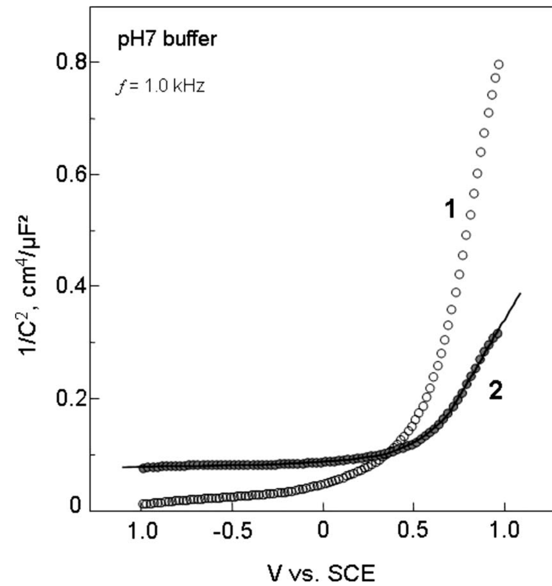

FIG. 5. Mott–Schottky plots of InN electrode in *p*H 7 buffer solution at 1 kHz oscillation frequency. The open symbols (1) as-grown surface, the closed symbols (2) after anodic oxidation. The solid curve (2) shows a MOS fit of the oxidized electrode.

rial with no charge transport across the interface. The nominal capacitance of the Q_2 element in the equivalent circuit, which is Q_0, was about 10 μF/cm^2. This value was in the range of the double layer capacitances measured on InAlN/GaN heterostructures.[14] The second circuit (R_2Q_2) can therefore be ascribed either to the electrochemical double layer or to a thin oxide layer on the as-grown surface as mentioned above. The parameters of the R_2Q_2 element remained nearly constant within the entire potential window in the electrolyte. This allowed us to extract the electronic characteristics of the surface from *C*-*V* measurements. At first, we derived the bias-dependent capacitance related to the InN layer. The high values of the resistances R_1 and R_2 enabled to simplify the equivalent circuit to two serial capacitances of a MOS structure,

$$C_1 = (1/C_P - 1/C_2)^{-1} \quad \text{and} \quad V_1 = V_{\mathrm{el}}C_2/(C_2 + C_{SC}), \quad (1)$$

where C_P is the overall capacitance taken at the electrode potential V_{el}. The capacitance C_2 was the nominal value of the CPE Q_2 equal to 10 μF/cm^2 as discussed above. The resulted Mott–Schottky plot $1/C_1^2$ versus V_1 is shown in Fig. 5, curve 1. The measurement was performed at $f=1$ kHz. The projected flatband potential using the data at high positive potentials was about +0.4 V versus SCE. The derived values of C_1 and V_1 were used to calculate the charge carrier profile on the surface layer of InN using the standard evaluation procedure for a metal-semiconductor interface. The resulting profile is shown in Fig. 6.

The point of equilibrium of the InN surface in the buffer electrolyte was determined by measuring the open circuit potential (OCP). The OCP value of the as-fabricated electrode was between 0.0 and −0.1 V versus SCE. In Fig. 5 this bias point corresponds to the depth of about 1.3 nm. The data in Fig. 6 show that most of the accumulated charge at the InN surface remained nondepleted at equilibrium. The density of the accumulated charge in equilibrium estimated from the *C*-*V* plot was about 2×10^{13} cm^{-2}. This value was in good agreement with the results of other reports on InN.[1,3] Analogous to Ref. 5, the extracted carrier profile was compared to the results of numerical simulation. In Fig. 5 it is shown by the solid curve. The simulated profile was obtained using SILVACO-ATLAS® device simulation software, which enables the self-consistent solution of the Poisson and Schrödinger equations.[24] The charge accumulation effect was modeled by locating a donor-type surface state in the con-

TABLE I. Fitting parameters of the electrochemical impedance spectra in Fig. 5 recorded at the electrode potential of +0.8 V versus SCE. The series resistance of the electrochemical cell was 10.5 Ω cm^2 for both cases.

	C_1 μF/cm^2	R_1 MΩ cm^2	Q_2: Q$_0$ μS sec^n/cm^2	Q_2: n	R_2 kΩ cm^2	Q_3: Q$_0$ μS sec^n/cm^2	Q_3: n	R_3 Ω cm^2
(a) As-grown surface	1.0	11.7	10.4	0.96	13.5	⋯	⋯	⋯
(b) Oxidized surface	3.0	0.74	2.5	0.87	0.77	19.9	0.75	59

Author complimentary copy. Redistribution subject to AIP license or copyright, see http://jap.aip.org/jap/copyright.jsp

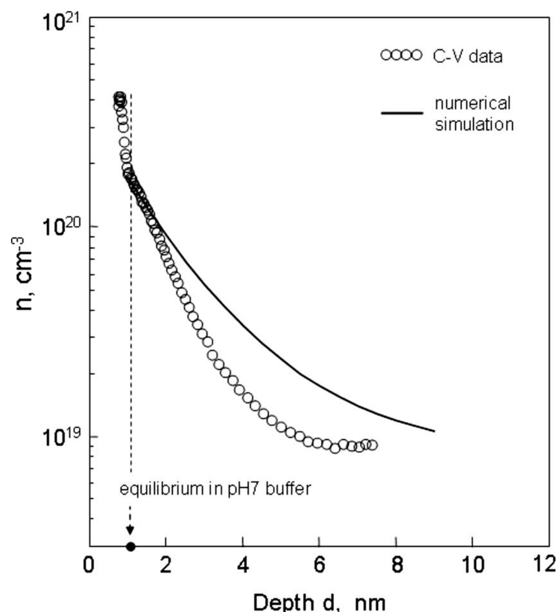

FIG. 6. Carrier profile in the as-grown InN derived from the capacitance-voltage data shown in Fig. 5 curve 1 (open symbols). The solid curve is the numerical simulation of the accumulation layer in InN. The black symbol on the *x*-axis shows the equilibrium point in contact with the electrolyte.

duction band of InN, according to the model description in Ref. 5. The profile calculated by the numerical solver was nearly identical to the theoretical data shown in Ref. 5. But in our case, a better agreement was found between the simulated curve and the *C-V* measurement. This may be due to the correction factor for the serial capacitance of the double layer in electrolyte [capacitance element C_2 in Eq. (1)]. The corresponding downward band bending at the InN surface was about 0.85 eV as obtained from the simulation.

Besides, the carrier concentration in the bulk InN extracted from the *C-V* plot was close to 9×10^{18} cm^{-3}, which is in agreement with the Hall effect measurements.

C. Oxidized InN in electrolyte

After the anodic oxidation treatment, the cyclic voltammogram of the InN surface showed an increase in background current in the potential window up to 10 nA/mm^2 at the positive potentials and a shift in the anodic current to higher potentials (curve 2 in Fig. 3). The increase in the background current appeared after polarizing the electrode into the range of hydrogen evolution and was similar to the current plateau observed for InP electrodes in the corresponding potential regime.[21,22] The shift in the oxygen evolution can be explained by the formation of the surface oxide layer, which leads to a potential distribution between depletion layer in InN and the oxide. However, the effect of the oxide layer on the onset of the oxygen evolution was less pronounced than, e.g., for InAlN/GaN heterostructures subjected to a similar oxidation process.[14] Besides, no significant shift in the hydrogen evolution corresponding to electron accumulation on the surface was observed. This may suggest that the formed oxide layer was transparent for the diffusion of ions. Such explanation is in agreement with the TEM data showing a porelike structure of the oxide [see Fig. 1(a)]. In case of a dense insulating layer a shift in the H evolution and a more pronounced shift in the O evolution would be expected due to the corresponding drops in potential.

The impedance spectrum of the oxidized surface is shown in Fig. 3(b) at the same potential of +0.8 V versus SCE. In this range of surface depletion the impedance data could be fitted by adding a parallel combination of CPE Q_2, resistance R_2, and a R_3Q_3 serial circuit to the R_1C_1 circuit describing the depletion layer in the as-grown case [Fig. 4(b), inset]. The fitting parameters are listed in Table I. Such an electrical equivalent circuit is typical for electrochemically active electrodes.[25] The CPE Q_2 might be related to the surface oxide. The dispersion factor n of Q_2 was 0.87, which could be explained by inhomogeneous characteristics of the surface.[26] However, the value of the nominal capacitance was about 2.5 $\mu\text{F}/\text{cm}^2$, as obtained from the fitting. This value would correspond to an oxide thickness of only 3.3 nm if one assumes a dielectric constant of 9.5 for a dense indium oxide[27] and which would be less than the average thickness of the oxide layer seen by TEM (see Fig. 1). On the other hand, the parallel resistance R_2 was only 0.7 $\text{k}\Omega\ \text{cm}^2$ compared to 14 $\text{k}\Omega\ \text{cm}^2$ related to the as-grown condition (see Table I). The low resistance across the oxide might be explained by the penetration of ions from the electrolyte through the porous oxide. In such a case the pores may also affect the dielectric constant of the oxide. The last elements R_3 and Q_3 of the equivalent circuit could be ascribed to the activity of the surface or the ion transfer through the oxide. The presence of chemically active sites on the oxidized surface would be in agreement with the increased background current observed in the corresponding cyclic voltammogram at positive potentials (curve 2 in Fig. 3), which is also supported by the results on indium and indium-phosphate electrodes in Refs. 20–22 mentioned above.

Due to the complicated equivalent circuit and the low parallel resistance, the *C-V* data of the oxidized electrode could not be evaluated using the same procedure as for the as-grown conditions by Eq. (1). Nevertheless, the Mott–Schottky plot of the oxidized InN shows the characteristic features of a MOS-like structure. The solid curve in Fig. 5 represents a fit of the measurement data by a standard MOS model. The fitting was made using a constant capacitance related to CPE Q_2 from the impedance spectroscopy in Fig. 4(b) and the doping concentration in InN layer of 9.6 $\times 10^{18}$ cm^{-3}. At negative potentials corresponding to the accumulation range, the *C-V* plot was limited to a constant capacitance of about 2.5 $\mu\text{F}/\text{cm}^2$, which might be attributed to the oxide layer. Note that the plotted capacitance in this case is the overall capacitance of the InN/indium oxide/electrolyte junction versus its electrode potential. The open-circuit potential of the oxidized surface was very close to that of the as-grown surface, approximately −0.1 V versus SCE in *p*H 7 buffer. This could be due to diffusion of ions through the porous oxide to the interface with InN, which shunts the potential drop across this layer. For that reason the barrier at the InN/oxide interface in equilibrium may not be determined from these measurements.

Author complimentary copy. Redistribution subject to AIP license or copyright, see http://jap.aip.org/jap/copyright.jsp

D. Planar resistor structure

The amount of fixed charge induced by oxidation was evaluated using the data on the planar resistor structure measured in air. Prior to oxidation, the sheet conductivity of the doped InN layer was about 30 mS, which corresponds to the Hall measurement data (see above). The main contribution to this conductivity was given by the doped bulk layer. The parallel conductivity along the surface accumulation layer σ_{surface} was estimated to about 0.3 mS by using the charge density n_s of 2×10^{13} cm^{-2} from Fig. 5. The corresponding carrier mobility in the surface accumulation layer was taken equal to 90 cm^2/V s using the data from literature.[6] After anodic oxidation, the sheet conductivity of the exposed InN area was reduced to 28 mS when measured in air. The drop by 2 mS was more than the expected reduction due to the surface accumulation layer. Therefore the reduction in conductivity may be related to three effects: (i) depletion of the surface accumulation layer, (ii) a reduction in InN layer thickness due to oxidation, and (iii) depletion of the remained bulk InN by fixed charge density at the InN/oxide interface.

The loss in InN bulk material by oxidation can be estimated using the TEM results, which revealed an average oxide thickness of about 10 nm with a porosity of ~50%. Then, a rough estimation of the lost InN bulk material would be about 5 nm. This would yield a reduction in the sheet conductivity by ~0.5 mS (using the bulk doping of 9.6 $\times10^{18}$ cm^{-3} and a carrier mobility of 650 cm^2/V s). The remaining part of 1.2 mS in this case could be ascribed to the effect of fixed charge at the InN/oxide interface. Using the bulk mobility, the value of 1.2 mS would correspond to a sheet charge of about 1.2×10^{13} cm^{-2}. Then, the total charge density needed to deplete both the surface accumulation layer and the bulk of InN would be about 3.1×10^{13} cm^{-2}. This high amount of charge could be related to the density of indium-oxide bonds at the oxidized interface and to a fixed charge inside the oxide layer.

E. Schottky diodes on the oxidized InN

More details on the surface depletion characteristics were obtained by analyzing the vertical metal diodes on the oxidized InN. The current-voltage (*I-V*) characteristic of a single diode structure with Ni/Au contact on the oxidized InN layer is shown in Fig. 7(a). The schematic cross section of the structure is shown in the inset. For comparison, the *I-V* curve between two Ni/Au contacts on the nonoxidized InN surface showed an Ohmic behavior with a resistance of 40 Ω for the same area of metal contacts.

The capacitance of the MOS diode was extracted from the results of impedance spectroscopy measurements performed in frequency range of 1 kHz–10 MHz at various bias points. The applied bias was limited to a range of −0.2 to +0.2 V due to leakage across the structure. At this bias range the impedance spectra were fitted by a single *RC*-circuit, as shown in the inset of Fig. 7(b). The fitting of the impedance spectra was made with the same software used to fit the electrochemical measurements discussed above. The plot of the parallel capacitance C_P extracted from the impedance

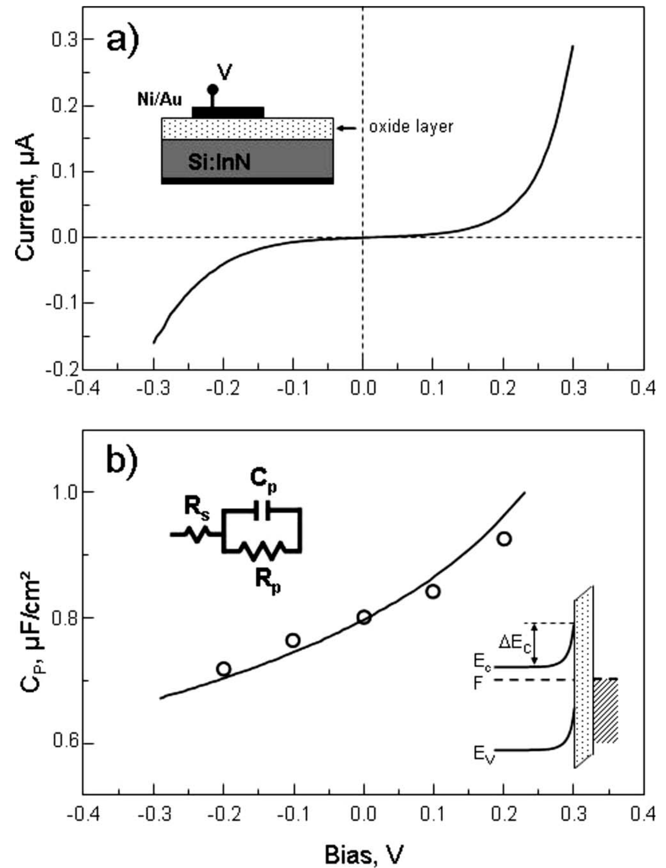

FIG. 7. (a) *I-V* characteristics of a Schottky diode on the oxidized InN (Ni/Au contact). The diameter of the metallization was about 100 μm. The schematic cross section of the diode structure is shown in the inset. (b) *C-V* plot of the diode capacitance derived from the impedance spectroscopy measurements at various biases. The equivalent circuit used for impedance spectroscopy analysis is shown in the inset. The solid curve is a MOS fit of the *C-V* data. A schematic cross section of the energy band diagram of the modeled structure is shown in the inset.

spectra versus the applied bias is shown in Fig. 7(b). The extracted *C-V* plot was compared to a model of an ideal MOS structure, which considers a series connection of the oxide capacitance and the capacitance across the surface depletion region. The values of the oxide capacitance and the InN doping were taken in the MOS model from measurements in the electrolyte. The oxide capacitance was set to 2.5 μF/cm^2 from the electrochemical impedance spectroscopy in Table I and which correlated also to the *C-V* plot in the electrolyte at negative potentials (see curve 2 in Fig. 5). The other fixed parameter in the MOS model was the background carrier concentration in the InN layer, which was set to 9.6×10^{18} cm^{-3} corresponding to the Hall measurement data and to the *C-V* measurements of the as-grown layer in the electrolyte (see Fig. 5). The best-matched simulation using these two fixed parameters is shown in Fig. 7(b) by the solid curve. The simulation curve corresponded to the upward band bending of the InN at the oxide interface with ΔE of about +0.5 eV. A schematic cross section of the modeled MOS structure at equilibrium is also shown in the inset of Fig. 7(b).

The concluded upward band bending correlated with the results on the planar resistor structure in Chap. 3.4, which

Author complimentary copy. Redistribution subject to AIP license or copyright, see http://jap.aip.org/jap/copyright.jsp

showed that the amount of oxidation-induced charge on the InN surface exceeded the electron density in the accumulation layer of the as-grown InN. It is also interesting to note that the electron affinity of InN $\chi=5.8$ (Ref. 28) and the work function of Ni metal $\phi_m=5.15$ would imply a surface accumulation layer in equilibrium, assuming an ideal MOS structure with no surface states at the InN/oxide interface and no fixed charge in the oxide layer. This again indicates that the anodic oxidation treatment of InN induces a large density of fixed charge depleting the surface accumulation layer. However, the origin of the oxidation-induced charge is not clear yet. It could be related to charged states at the oxide interface or to a fixed charge within the oxide layer.

IV. CONCLUSION

In this paper we have attempted to investigate the surface morphology and the electronic characteristics of Si-doped InN layers subjected to anodic oxidation in 0.1 M KOH electrolyte. The epitaxial layers of InN were grown on *c*-sapphire substrate and GaN buffer and AlN interlayer. It was shown that the applied treatment resulted in a surface oxide layer. TEM disclosed an oxide, which was nonuniform in thickness and morphology. The growth of the oxide layer occurred preferentially in the regions of troughs in the faceted initial surface, which could be associated with dislocations emerging at these sites. The TEM images revealed a porous structure of the produced oxide layer. The pores varied from 1 to 5 nm in diameter and were observed both at surface facets and in the regions of troughs throughout the entire thickness of the oxide. Fourier spectrum from the oxide area revealed reflections of crystalline In_2O_3 phase.

The porous structure of the anodic oxide might be linked to a leakage across the MOS diodes fabricated on the oxidized InN. This high leakage still prevents to use such oxide layers as the gate insulator of InN-based MOSFET devices. Nevertheless, the applied anodic treatment depleted the accumulation charge of the as-grown InN surface and induced an upward band bending at the InN/oxide interface. The value of the upward band bending was estimated to about 0.5 eV from modeling the capacitance-voltage characteristics of the MOS diodes. In comparison, the analysis of the same InN layers prior to the oxidation revealed the downward band bending with the corresponding density of the accumulated electron charge of 2×10^{13} cm^{-2}. The density of the oxidation-induced charges was estimated to be $\sim3\times10^{13}$ cm^{-2} from the analysis of planar resistor structures on the InN surface and which would be sufficient to deplete the surface accumulation charge.

[1]H. Lu, W. J. Schaff, L. F. Eastman, and C. F. Stutz, Appl. Phys. Lett. **82**, 11 (2003).
[2]L. Colakerol, T. D. Veal, H. K. Jeong, L. Plucinski, A. DeMasi, T. Learmonth, P. A. Glans, S. Wang, Y. Zhang, L. F. Piper, P. H. Jefferson, A. Fedorov, T. C. Cheng, T. D. Moustakas, C. F. McConville, and K. Smith, Phys. Rev. Lett. **97**, 237601 (2006).
[3]V. Cimalla, M. Niebelschütz, G. Ecke, V. Lebedev, O. Ambacher, M. Himmerlich, S. Krischok, J. A. Schaefer, H. Lu, W. J. Schaff, Phys. Status Solidi A **203**, 59 (2006).
[4]T. D. Veal, I. Mahboob, L. F. J. Piper, C. F. McConville, H. Lu, and W. J. Schaff, J. Vac. Sci. Technol. B **22**, 2175 (2004).
[5]I. Mahboob, T. D. Veal, L. F. Piper, C. F. McConville, H. Lu, W. J. Schaff, J. Furthmueller, and F. Bechstedt, Phys. Rev. B **69**, 201307 (2004) (R).
[6]H. Lu, W. J. Schaff, and L. F. Eastman, J. Appl. Phys. **96**, 3577 (2004).
[7]Y. S. Lu, C. C. Huang, J. A. Yeh, C. F. Cheng, and S. Gwo, Appl. Phys. Lett. **91**, 202109 (2007).
[8]Y. S. Lin, S. H. Koa, C. Y. Chan, S. S. H. Hsu, H. M. Lee, and S. Gwo, Appl. Phys. Lett. **90**, 142111 (2007).
[9]M. A. Garcia, S. D. Wolter, T. H. Kim, S. Choi, M. Losurdo, and G. Bruno, Appl. Phys. Lett. **88**, 013506 (2006).
[10]D. J. Fu, Y. H. Kwon, T. W. Kang, C. J. Park, K. H. Baek, H. Y. Cho, D. H. Shin, C. H. Lee, and K. S. Chung, Appl. Phys. Lett. **80**, 3 (2002).
[11]V. Cimalla, V. Lebedev, C. Y. Wang, M. Ali, G. Ecke, V. M. Polyakov, F. Schwierz, O. Ambacher, H. Lu, and W. J. Schaff, Appl. Phys. Lett. **90**, 152106 (2007).
[12]V. Lebedev, C. J. Wang, V. Cimalla, S. Hauguth, T. Kups, M. Ali, G. Ecke, M. Himmerlich, S. Krischok, J. A. Schaefer, O. Ambacher, V. M. Polyakov, and F. Schwierz, J. Appl. Phys. **101**, 123705 (2007).
[13]T. Rotter, D. Mistele, J. Stemmer, F. Fedler, J. Aderhold, J. Graul, V. Schwegler, C. Kirchner, J. Kamp, and M. Heuken, Appl. Phys. Lett. **76**, 3923 (2000).
[14]C. Pietzka, A. Denisenko, M. Alomari, F. Medjdoub, J. F. Carlin, E. Feltin, N. Grandjean, and E. Kohn, J. Electron. Mater. **37**, 616 (2008).
[15]N. Asai, Y. Inoue, H. Sugimura, and O. Takai, J. Electrochem. Soc. **146**, 2365 (1999).
[16]W. J. Schaff, H. Lu, L. F. Eastman, W. Walukiewicz, K. M. Yu, S. Keller, S. Kurtz, B. Keyes, and L. Gevilas, ECS Meeting, Proceedings in State-of-the-Art Program on Compound Semiconductors XLI and Nitride and Wide Bandgap Semiconductors for Sensors, Photonics, and Electronics, edited by V. H. Ng and A. G. Baca, 2004, Vol. 2004–06 (unpublished).
[17]U. Kaiser, A. Chuvilin, P. D. Brown, and W. Richter, Microsc. Microanal. **5**, 420 (1999).
[18]A. Pakes, P. Skeldon, G. E. Thompson, J. W. Fraser, S. Moisa, G. I. Sproule, M. J. Graham, and S. B. Newcomb, J. Mater. Sci. **38**, 343 (2003).
[19]C. Youtsey, I. Adesida, and G. Bulman, Appl. Phys. Lett. **71**, 2151 (1997).
[20]S. Omanovic and M. Metikos-Hukovic, J. Appl. Electrochem. **27**, 35 (1997).
[21]J. Vigneron, M. Herlem, E. M. Koumri, and A. Etcheberry, Appl. Surf. Sci. **201**, 51 (2002).
[22]A. Gagnaire, J. Joseph, and A. Etcheberry, J. Electrochem. Soc. **134**, 2475 (1987).
[23]T. Hashizume, S. Ootomo, R. Nakasaki, S. Oyama, and M. Kihara, Appl. Phys. Lett. **76**, 2880 (2000).
[24]*ATLAS User's Manual. Device Simulation Software* (Silvaco Inc., Santa Clara, CA, 2003).
[25]J. R. Macdonald, *Impedance Spectroscopy* (Wiley, New York, 1987).
[26]C.-H. Kim, S.-I. Pyun, and J.-H. Kim, Electrochim. Acta **48**, 3455 (2003).
[27]W. Walukiewicz, J. W. Ager, K. M. Yu, Z. Liliental-Weber, J. Wu, S. X. Li, R. E. Jones, and J. Denlinger, J. Phys. D **39**, R83 (2006).
[28]M. E. Levinshtein, S. L. Rumyantsev, and M. S. Shur, *Properties of Advanced Semiconductor Materials GaN, AlN, SiC, BN, SiG* (Wiley, New York, 2001).

Author complimentary copy. Redistribution subject to AIP license or copyright, see http://jap.aip.org/jap/copyright.jsp